Soft Matter

PAPER

Cite this: *Soft Matter*, 2018, **14**, 7526

Effect of graphene on the absorption of methanol and crack healing in poly(methyl methacrylate)-based composites

Zu-wen Lin,[a] Fuqian Yang [b] and Sanboh Lee *[a]

Received 16th July 2018,
Accepted 15th August 2018

DOI: 10.1039/c8sm01454j

rsc.li/soft-matter-journal

This work is focused on the mass transport of methanol and the methanol-assisted crack healing in poly(methyl methacrylate) (PMMA)–graphene composites at different temperatures. The effect of the fraction of graphene on the mass transport of methanol and the methanol-assisted crack healing is also studied. The experimental results reveal that adding graphene to the PMMA matrix increases the resistance to the migration/diffusion of methanol and polymer chains in the PMMA matrix, and the absorption of methanol follows anomalous diffusion. The activation energies for the case I transport and case II transport in the PMMA–graphene composites are relatively independent of the fraction of graphene, and are larger than the corresponding ones in pure PMMA. Increasing the healing time and healing temperature allows for more polymer chains to migrate/diffuse across fractured surfaces, leading to the increase in the fracture strength of the crack-healed PMMA–graphene composites.

Introduction

Graphene as a two-dimensional, one-atom-thick sheet with sp^2 bonded carbon atoms has attracted great interest due to potential applications in electronics,[1,2] photonics,[3,4] polymer-based composites,[5–7] *etc.* In the heart of the potential applications are the unique properties of graphene, including high Young's modulus, fracture strength, and mobility of charge carriers.

There are extensive studies focusing on the mechanical behaviour of polymer–graphene nanocomposites.[8–11] Using solution mixing and compression moulding, Gupta *et al.*[9] prepared polymer-based conductive nanocomposites consisting of ultra-high molecular weight polyethylene (UHMWPE), carbon nanotubes (CNTs) and graphene nanoplatelets (GNP), and found that the elastic modulus and yield strength of the nanocomposites with 0.1/0.3 wt% of CNT/GNP are 37% and 33% more than the elastic modulus and yield strength of pure UHMWPE, respectively. Melt-blending polypropylene (PP) with graphite nanosheets (GN), Rosehr *et al.*[10] formed PP–GN composites, and demonstrated that GN increases the yield strength of the composites by 20%. Zhang *et al.*[11] used three-dimensional interconnected graphene foam (GF) and poly(methyl methacrylate) (PMMA) to form PMMA–GF composites with 0.4 wt% graphene *via* an *in situ* polymerization method, and found that GF increases the local mechanical strength of the composite. Li *et al.*[12] studied the mechanical properties of polymer composites reinforced by CNTs and graphene sheets; their results showed that the graphene sheets improve the mechanical strength of the composites. Rafiee *et al.*[13] observed that graphene fillers are effective in suppressing the crack propagation in epoxy polymers. However, there is little study on the effect of graphene on the crack healing in polymers. It is worth pointing out that there are studies on the use of stimuli-responsive nanostructures to induce self-healing of polymer coatings for the corrosion protection of metal.[14–16]

It is known that the diffusion of solvents in a polymer can cause the structure change of the polymer, leading to local swelling/softening[17–21] and/or crack healing.[22–25] Recently, there are reports on the swelling behaviour of polymer–CNT composites[26–30] for the potential application of the polymer–CNT composites in liquid sensing. None of these studies have examined the effect of graphene on the swelling behaviour of polymers and the crack healing in polymers due to the absorption/diffusion of solvents. With the potential applications of polymer–graphene composites in a variety of areas, it is of great importance to investigate the physical and mechanical behaviour of polymer–graphene composites. In this work, we study the absorption of methanol and the methanol-assisted crack healing in PMMA–graphene composites. The effects of the fraction of graphene on the absorption of methanol and the crack healing are examined.

[a] *Department of Materials Science and Engineering, National Tsing Hua University, Hsinchu 300, Taiwan. E-mail: sblee@mx.nthu.edu.tw; Fax: +886-3-5719677; Tel: +886-3-5719677*

[b] *Department of Chemical and Materials Engineering, University of Kentucky, Lexington, KY 40506, USA*

Methodology

Assuming that the diffusion/absorption of solvent in a polymer plate of 2ℓ in thickness involves Case I and Case II transport, Harmon *et al.*[31] solved the one-dimensional diffusion problem with a constant solvent concentration of C_0 at surfaces ($x = 0$ and $x = 2\ell$) and obtained the spatiotemporal evolution of the solvent concentration of C in the polymer plate as

$$\frac{C(x,t)}{C_0} = 1 - 2e^{vx/2D}\sum_{n=1}^{\infty}\frac{\lambda_n \sin(\lambda_n x/\ell)}{\beta_n^2\left(1+\frac{2D}{v\ell}\cos^2\lambda_n\right)}e^{-\beta_n^2 Dt/\ell^2} \quad (1a)$$

with

$$\lambda_n = \frac{v\ell}{2D}\tan\lambda_n \text{ for } 0 < x < \ell, \quad (1b)$$

and

$$\frac{C(x,t)}{C_0} = 1 - 2e^{(v/2D)(2\ell-x)}\sum_{n=1}^{\infty}\frac{\lambda_n \sin(\lambda_n(2\ell-x)/\ell)}{\beta_n^2\left(1+\frac{2D}{v\ell}\cos^2\lambda_n\right)}e^{-\beta_n^2 Dt/\ell^2} \quad (2a)$$

with

$$\lambda_n = \frac{-v\ell}{2D}\tan\lambda_n \text{ for } \ell < x < 2\ell, \quad (2b)$$

where

$$\beta_n^2 = \frac{v^2\ell^2}{4D^2} + \lambda_n^2 \quad (3)$$

Here, D and v are the diffusivity and the velocity associated with the diffusion/absorption of solvent for the Case I and Case II transport, respectively, and λ_n ($n = 1, 2, \ldots$) are the positive eigenvalues determined by eqn (2b). Note that the direction of velocity for Case II transport is toward the specimen centre. The temporal evolution of the amount of solvent per unit area absorbed in the polymer plate is found by the integration of the solvent concentration, eqn (1a) and (2a), over the thickness of the polymer plate as

$$\frac{M}{M_\infty} = 1 - 2\sum_{n=1}^{\infty}\frac{\lambda_n^2\left(1-2\cos\lambda_n e^{v\ell/2D}\right)}{\beta_n^4\left(1+\frac{2D}{v\ell}\cos^2\lambda_n\right)}e^{-\beta_n^2 Dt/\ell^2} \quad (4a)$$

Here,

$$M_\infty = \lim_{t\to\infty} M = 2\ell C_0. \quad (4b)$$

It is known that the absorption of a solvent in a polymer plate is a thermally activated process, involving the diffusion/migration of the solvent and the interdiffusion of polymer chains. The temperature-dependence of D and v can be described by the Arrhenius relation as

$$D = D_0 e^{-Q_D/RT} \text{ and } v = v_0 e^{-Q_v/RT} \quad (5)$$

where D_0 and v_0 are the corresponding pre-exponential factors, R is the gas constant, T is absolute temperature, and Q_D and Q_v are the activation energies for the case I transport and case II transport, respectively.

The equilibrium swelling ratio (ESR), which is calculated as the ratio of the equilibrium mass of absorbed solvent to the mass of the specimen without the absorption of the solvent, is associated with the affinity and exchange of enthalpy between the polymer and the solvent. In general, the temperature-dependence of the ESR can be described by the van't Hoff's equation as[26]

$$\text{ESR} = (\text{ESR})_0 e^{-\Delta H/RT} \quad (6)$$

with $(\text{ESR})_0$ being a pre-exponential factor, and ΔH being the mixing heat for the absorption process.

For the solvent-assisted crack healing, Lin *et al.*[32] suggested that the temporal evolution of the length of a crack, a, in a polymer can be expressed as

$$a = a_0 - \frac{\alpha D\gamma}{RT}t \equiv a_0 - Vt \quad (7)$$

where a_0 is the initial length of the crack, γ is the specific surface energy of the polymer, α is a characteristic length, and V is the crack closure rate. The proportionality between V and D/T, as given in eqn (7), suggests that the temperature-dependence of VT can be described by the Arrhenius relationship.

Experimental details

Solution mixing with the solvent tetrahydrofuran (THF) was used to fabricate PMMA–graphene composites. PMMA powder with an average molecular weight of ~120 000, as measured by GPC (gel permeation chromatography), and functionalized graphene (–COOH) were obtained from Aldrich (St. Louis, MO 63178, United States) and from Euflex Technology Corp. (New Taipei City, Taiwan), respectively. Tetrahydrofuran and methanol were purchased from ECHO CHEMICAL CO. (Miaoli County, Taiwan). Note that there are various methods available for the functionalization of graphene.[33] The functionalization of graphene with carboxyl groups generally involves the decomposition of nitric acid induced by graphene clusters to nitrogen oxides and the reactive hydroxyls and sequential hydroxyl attack at the active sites of carbon to form carboxyl groups.[34]

The as-received PMMA powder was first dried in a vacuum oven at 80 °C to remove the water absorbed in the PMMA powder. 10 g of dried PMMA powder was then dissolved in 100 ml of THF (the density of THF is 0.89 g ml^{-1}) under mechanical stirring to form a transparent solution of 10 wt% PMMA. Functionalized graphene (–COOH) of different amounts was placed in 10 ml of THF to form a suspension, which was then mixed with the PMMA/THF solution. The mixture of the suspension and the solution was sonicated at room temperature for 1.5 h to form a homogeneous suspension. The homogeneous suspension was dripped into 600 ml of methanol to allow the precipitation of small particles, which were collected by suction filtration through a PTFE (poly(tetrafluoroethylene)) membrane. The collected particles were dried at 50 °C in a vacuum oven for 24 h. The dried

particles were then mechanically ground to form PMMA/graphene powder.

PMMA–graphene composites were fabricated *via* hot pressing of PMMA/graphene powder. The PMMA/graphene powder, which filled a mould of 1 mm in thickness, was hot-pressed at 180 °C by a C Carver 3851 hot press machine (Wabash, IN, USA) for 10 min under the action of 2 MPa.

Specimens of rectangular cuboids with dimensions of $5 \times 5 \times 1$ mm^3 were made from the PMMA–graphene composites. The specimens were mechanically ground subsequently on emery papers of 400, 800, 1200, and 2000 grit, and then polished with alumina slurries of 1 μm and 0.05 μm, consecutively. All the polished specimens were annealed at 90 °C in air for 24 h to release the residual stresses in the specimens.

Methanol was used in the study of the absorption behaviour of the PMMA–graphene composites at different temperatures. A glass container with methanol was placed in a water bath, which was maintained at a pre-set temperature. Specimens were immersed in the methanol, and temporal variations of the weights of the specimens were measured regularly on an analytical balance (OHAUS-AP250D, New Jersey, USA).

The methanol-assisted healing of the cracks in PMMA–graphene composites was performed at different temperatures. Following the same process of the sample preparation for the absorption of methanol, specimens with dimensions of $2 \times 1 \times 0.1$ cm^3 were prepared. A single crack/notch of 0.1 mm in length was introduced to the specimens at the central section by a blade. The cracked specimens, which were heated first to a pre-set temperature, were immersed in methanol of the same temperature in the range of 40–55 °C. A digital camera was used to record the evolution of the crack length, which was analysed by the software ImageJ. For each condition, three tests were performed, and the results reported were the average of the three tests.

The tensile test of the crack-healed specimens with the dimensions shown in Fig. 1 was performed at room temperature on a universal tensile machine (INSTRON 4468, Norwood, MA). After nearly complete removal of the methanol residue absorbed in the specimens with the healed crack in air, the specimens were machined to tensile bars without the presence of any visible cracks. The displacement-control mode was used for the tensile tests, and the crosshead speed was 16.7 μm s^{-1}. The fracture strength was calculated from the stress–strain curves.

Raman spectroscopy measurement was performed to study the effects of graphene and methanol on the chemical bonds of PMMA and PMMA–graphene composites using a LABRAM HR800 UV confocal micro-Raman spectrometer (Horiba, Kyoto, Japan). The standard point mapping in the Raman imaging mode with a high-power helium-neon laser (λ = 632.8 nm) was used with the wavenumber in the range of 700 to 3800 cm^{-1}.

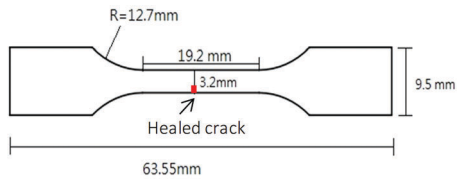

Fig. 1 Geometrical dimensions of tensile specimens.

Results and discussion

Fig. 2 shows the Raman spectra of the PMMA–graphene composites with different fractions of graphene. It is evident that all the composites exhibit the peaks at wavenumbers of 1326 cm^{-1} and 1583 cm^{-1}, whose intensities increase with the increase of the fraction of graphene. In addition, adding graphene to PMMA led to the presence of a peak at a wavenumber of 2678 cm^{-1}. The three peaks at 1326, 1583 and 2678 cm^{-1} correspond to the D band, G band, and 2D band of graphite, respectively. The D band represents the stacking disorder between two layers and atomic defects within the layer, the G band is associated with the longitudinal optical (LO) phonon mode and the graphitic structure, and the 2D band is attributed to the second resonance of C atoms by sp^2 binding.[35] The functional group of –COOH attached to the graphene introduces defects and makes the D band detectable.

It is known that the wavenumber of the G band is dependent on the number of graphene layers, and the G band of single layer graphene has a wavenumber of 1587 cm^{-1}. From Fig. 2, we note that there is a blueshift of the G band from 1569 cm^{-1} to 1583 cm^{-1}, which suggests that increasing the fraction of graphene in the PMMA leads to the reduction of the number of graphene layers, *i.e.* the graphene is presented in the exfoliated form.

The intensity ratio of the D band to the G band represents the degree of the defects in the graphene structure. Using the peak intensities, the intensity ratio of the D band to the G band is found to decrease with the increase of the fraction of graphene in PMMA, implying that the interaction between PMMA and graphene reduces the degree of the defects in the graphene structure.

Fig. 3 shows the temporal evolution of the amount of methanol absorbed in the PMMA–graphene composites with 0.1 wt% of graphene at different temperatures (Fig. 3a) and

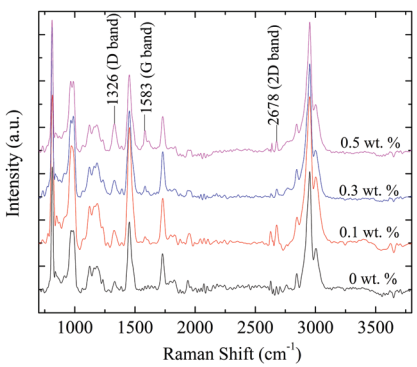

Fig. 2 Raman spectra of PMMA–graphene composites with different fractions of graphene.

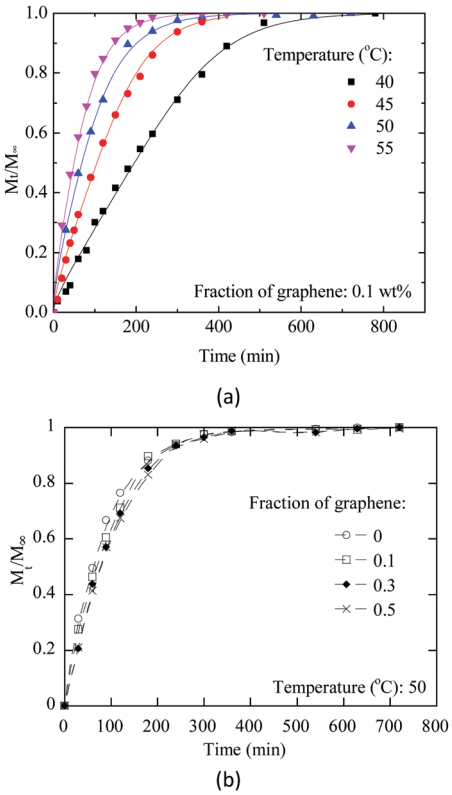

Fig. 3 Temporal evolution of the amount of methanol absorbed in PMMA–graphene composites: (a) for different temperatures with 0.1 wt% of graphene, and (b) for different fractions of graphene at 50 °C.

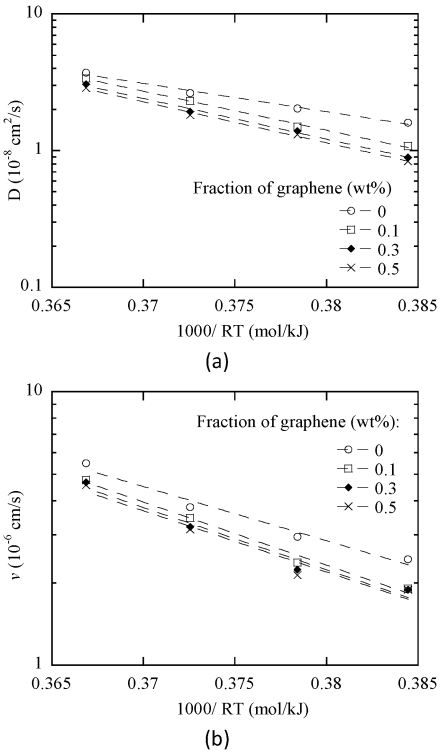

Fig. 4 Temperature dependence of (a) D and (b) v for PMMA–graphene composites with different weight fractions of graphene.

with different fractions of graphene at 50 °C (Fig. 3b). It is evident that the amount of methanol absorbed in the PMMA–graphene composites increases with increasing the absorption time. Increasing the absorption temperature leads to the increase of the absorption of methanol in the PMMA–graphene composites, as shown in Fig. 3a, suggesting the decrease of the resistance to the migration/diffusion of methanol in the PMMA–graphene composites and the increase of the migration/diffusion rate of methanol with the increase of temperature.

For the same absorption temperature and time, the PMMA–graphene composite without graphene generally has the largest relative amount of methanol (M_t/M_∞), and the PMMA–graphene with 0.5 wt% of graphene generally has the smallest relative amount of methanol. Such a trend reveals that the resistance to the migration/diffusion of methanol in the PMMA–graphene composites increases with the increase of the fraction of graphene due to the strong interaction between PMMA and graphene, as supported by the decrease of the intensity ratio of the D band to the G band with the increase of the fraction of graphene in PMMA.

Using eqn (4), we curve-fit the experimental data, including the data shown in Fig. 3. For comparison, the fitting results are also depicted in Fig. 3. It is evident that eqn (4) well describes the absorption of methanol in the PMMA–graphene composites for the temperature range and the weight fractions of graphene used in this work. The behaviour of the migration/diffusion of methanol in the PMMA–graphene composites can be described by the abnormal transport involving the Case I and Case II transport. Note that there are two fitting parameters of D and v in eqn (4), which are temperature-dependent.

Fig. 4 shows the temperature dependence of D and v for the PMMA–graphene composites with different weight fractions of graphene. Both D and v increase with the increase of temperature, as expected, since the parameter D represents the rate of the migration/diffusion of methanol in PMMA, and v is dependent on the migration/diffusion of polymer chains. It is expected that both processes can be described by the Arrhenius relationship of eqn (5). Using eqn (5), we curve-fit the data given in Fig. 4. For comparison, the fitting curves are also included in Fig. 4. It is evident that the Arrhenius relationship of eqn (5) indeed can be used to describe the temperature dependence of D and v, suggesting that the methanol absorption in the PMMA–graphene is a thermal activation process involving two rate processes.

From Fig. 4, we note that both D and v decrease with the increase of the fraction of graphene. Generally, both D and v are proportional to the mobility of the corresponding species, which is inversely proportional to the resistance to the migration/diffusion of the species. Increasing the fraction of graphene in PMMA leads to the increase in the interaction between polymer chains and graphene, resulting in the increase of the resistance to the migration/diffusion of methanol and polymer chains in the PMMA–graphene composites.

Using the results from the curve-fitting of the data in Fig. 4, the activation energies for the migration/diffusion of methanol

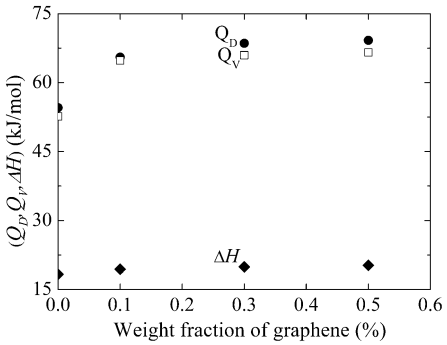

Fig. 5 Variation of activation energies and mixing heat with the fraction of graphene in PMMA–graphene composites.

and polymer chains in the PMMA–graphene with different fractions of graphene are depicted in Fig. 5. It is evident that the activation energies of Q_D and Q_v for the PMMA–graphene composites with graphene are larger than the corresponding ones for the PMMA without graphene, and both the activation energies are relatively independent of the fraction of graphene used in this work. The larger activation energies of Q_D and Q_v for the PMMA–graphene composites with graphene than the corresponding ones for the PMMA without graphene confirm the interaction between graphene and polymer chains, which causes the change of the absorption of methanol in the PMMA–graphene composites.

Fig. 6 shows the temperature dependence of the maximum absorption of methanol in the PMMA–graphene composites with different weight fractions of graphene. At the same temperature, pure PMMA has the smallest ESR, and there is no significant difference in the ESRs between the PMMA–graphene composites. Such a trend suggests that the graphene in the PMMA matrix likely introduces local loose structures/pores around graphene, which allows more methanol to be absorbed in the PMMA–graphene composites. Using eqn (6), we curve-fit the data in Fig. 6 and obtain the mixing heat (ΔH), which is shown in Fig. 5. The mixing heat of pure PMMA is smaller than those of the PMMA–graphene composites, and the mixing heat of the PMMA–graphene composites is relatively independent of the fraction of graphene used in this work.

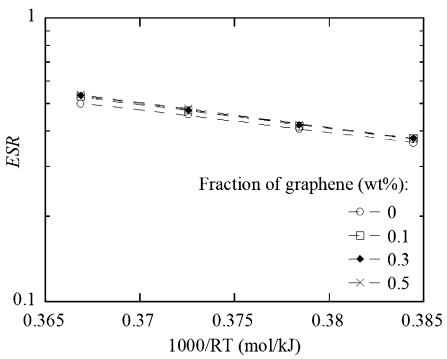

Fig. 6 Temperature dependence of the ESR for the absorption of methanol in PMMA–graphene composites with different weight fractions of graphene.

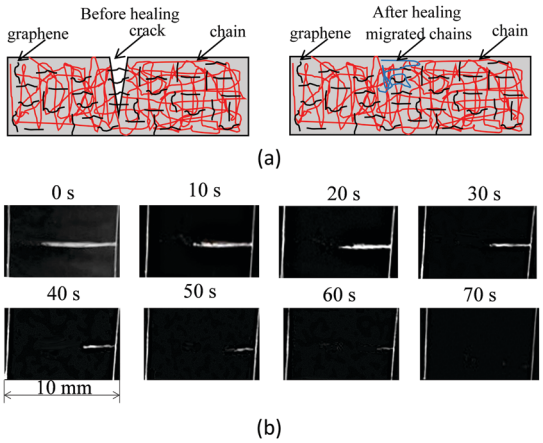

Fig. 7 (a) Schematic of crack healing with penetration of polymer chains through crack surfaces, and (b) optical images of the size of a crack in a pure PMMA at different times in methanol at a temperature of 50 °C.

It is known that solvent can accelerate the migration/diffusion of polymer chains across interfaces, leading to the closure of cracks in a polymer, as schematically shown in Fig. 7a. Fig. 7b shows optical images of the size of a crack indicated by the white zone in pure PMMA at different times in methanol at a temperature of 50 °C. It is evident that the size of the crack decreases with the increase of the immersion time, revealing the methanol-assisted crack healing in PMMA, and the crack eventually closed/healed. From the optical images, we have calculated the healing speed of the crack, and the result shows that the closure of the crack progressed at an approximately constant speed. All the cracked PMMA–graphene samples, which were immersed in methanol in a temperature range of 40–55 °C, exhibited similar behaviour, *i.e.* the sizes of all the cracks decrease approximately linearly with the immersion time. It is worth pointing out that pure PMMA is transparent and the PMMA–graphene composite is black. The optical image of the crack indicated by a white zone in pure PMMA is not easy to observe in the PMMA–graphene composites because of the low contrast between the specimen and the crack.

As shown in eqn (7), the closure speed of a crack in a polymer in a solvent is proportional to the diffusivity of polymer chains, which is temperature-dependent. Fig. 8 shows the temperature dependence of VT for the crack healing in all the cracked PMMA–graphene specimens in methanol. The product of VT increases with the increase of temperature, as expected. Using the Arrhenius relation for VT to fit the data shown in Fig. 8, we obtain the activation energies for the crack healing in the PMMA–graphene composites as 56.9, 66.0, 67.5 and 69.9 kJ mol^{-1} for the PMMA–graphene composites with graphene fractions of 0, 0.1, 0.3, and 0.5, respectively. The activation energies for the PMMA–graphene composites with graphene fractions of 0.1, 0.3, and 0.5 are comparable with 65.8, 68.5 and 69.2 kJ mol^{-1} for the migration/diffusion of methanol in the corresponding composites, and the activation energy of 56.9 kJ mol^{-1} for pure PMMA is comparable to 54.5 kJ mol^{-1} for the migration/diffusion of methanol in pure PMMA. Such a trend suggests that the migration/diffusion of methanol in the

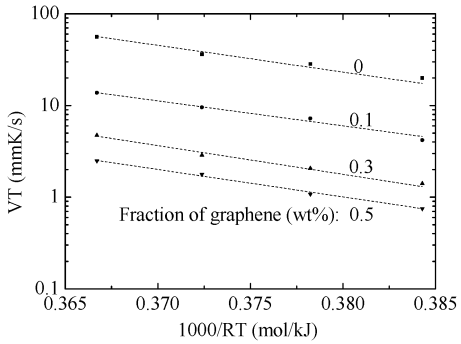

Fig. 8 Temperature-dependence of *VT* for the crack healing in PMMA–graphene composites.

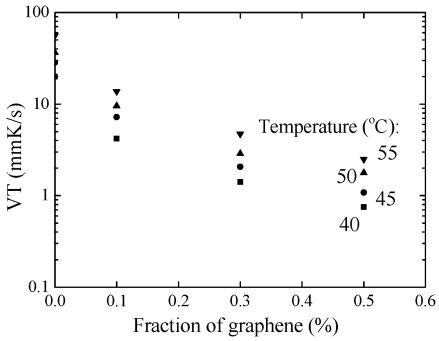

Fig. 9 Variation of *VT* with the weight fraction of graphene in PMMA–graphene at different temperatures.

PMMA–graphene composites plays an important role in the crack healing, and the crack surface in pure PMMA also plays a role in regulating the migration/diffusion of polymer chains for the crack healing. Note that Lin *et al.*[32] also observed similar behaviour in pure PMMA of large molecular weight, and obtained an activation energy of 125 kJ mol^{-1} for the crack closure. Increasing molecular weight leads to the increase of the energy barrier for the diffusion/migration of polymer chains.

Fig. 9 shows the variation of *VT* with the weight fraction of graphene in the PMMA–graphene composites at different temperatures. At the same temperature, the healing speed of a crack decreases nonlinearly with the increase of the fraction of graphene, suggesting that adding graphene increases the resistances to the migration/diffusion of methanol and polymer chains. It is the combined effect of methanol and the migration/diffusion of polymer chains that determines the crack healing in the PMMA–graphene composites.

Fig. 10 shows the variation of the fracture strength of the crack-healed PMMA–graphene composites with healing time for different fractions of graphene. The fracture strength of the crack-healed PMMA–graphene composites increases with the increase of the healing time, as expected. Increasing the healing time allows more polymer chains to migrate/diffuse across the cracked surfaces to increase the bonding strength of the fractured surfaces. From Fig. 10, we also note that the

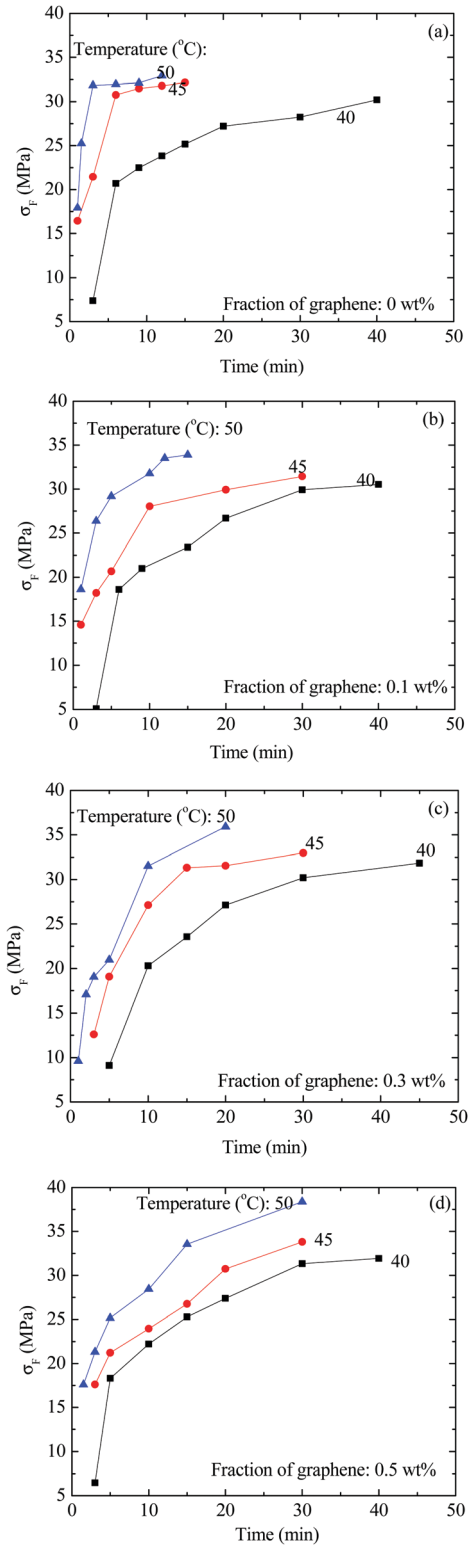

Fig. 10 Variation of fracture strength with healing time for crack-healed PMMA–graphene composites with different fractions of graphene at three different temperatures: (a) 0 wt%, (b) 0.1 wt%, (c) 0.3 wt%, and (d) 0.5 wt%.

fracture strength increases with the increase of the healing temperature for the same healing time. Such a trend is due to the fact that the migration/diffusion of polymer chains is a

thermally activated process, whose rate increases with the increase of temperature. Increasing the healing temperature helps polymer chains across the fractured surfaces at relatively high speed, and there are more polymer chains across the fractured surfaces at a higher temperature than at a lower temperature for the same healing time.

Conclusions

In summary, we have used solution mixing to prepare PMMA–graphene composites with different fractions of graphene. Considering the potential applications of polymer–graphene composites, we have investigated the absorption of methanol in the prepared PMMA–graphene composites and the methanol-assisted crack healing in the PMMA–graphene composites. The following is a summary of the main results.

(1) Increasing the fraction of graphene in PMMA leads to the reduction of the number of graphene layers.

(2) The absorption of methanol in the prepared PMMA–graphene composites follows anomalous diffusion. Adding graphene to PMMA increases the energy barriers needed for the migration/diffusion of methanol and polymer chains in the PMMA.

(3) The activation energies for the migration/diffusion of methanol and polymer chains in the PMMA–graphene composites are larger than the corresponding ones for pure PMMA, and both the activation energies are relatively independent of the fraction of graphene used in this work.

(4) Pure PMMA has the smallest ESR, and there is no significant difference in the ESRs between the PMMA–graphene composites.

(5) All the cracked PMMA–graphene samples after being immersed in methanol in a temperature range of 40–55 °C exhibit similar behaviour, *i.e.* the sizes of all the cracks decrease linearly with the immersion time.

(6) The activation energies for the PMMA–graphene composites with graphene fractions of 0.1, 0.3, and 0.5 are comparable with the corresponding ones for the Case I transport of methanol in the corresponding composites.

(7) The fracture strength of the crack-healed PMMA–graphene composites increases with the increase of the healing time and the healing temperature.

Conflicts of interest

There are no conflicts to declare.

Acknowledgements

This work was financially supported by the Ministry of Science and Technology, Taiwan through the grant MOST107-2221-E-007-007-MY2. FY is grateful for the support by the NSF through the grant CMMI-1634540, monitored by Dr Khershed Cooper.

References

1 X. Wang, Y. Ouyang, X. Li, H. Wang, J. Guo and H. Dai, *Phys. Rev. Lett.*, 2008, **100**, 206803.
2 H. A. Becerril, J. Mao, Z. Liu, R. M. Stoltenberg, Z. Bao and Y. Chen, *ACS Nano*, 2008, **2**, 463–470.
3 F. Bonaccorso, Z. Sun, T. Hasan and A. Ferrari, *Nat. Photonics*, 2010, **4**, 611.
4 Q. Bao and K. P. Loh, *ACS Nano*, 2012, **6**, 3677–3694.
5 S. Stankovich, D. A. Dikin, G. H. Dommett, K. M. Kohlhaas, E. J. Zimney, E. A. Stach, R. D. Piner, S. T. Nguyen and R. S. Ruoff, *Nature*, 2006, **442**, 282.
6 B. Debelak and K. Lafdi, *Carbon*, 2007, **45**, 1727–1734.
7 R. Sengupta, M. Bhattacharya, S. Bandyopadhyay and A. K. Bhowmick, *Prog. Polym. Sci.*, 2011, **36**, 638–670.
8 V. Mittal and V. Mittal, Polymer–graphene nanocomposites. *RSC Nanoscience & Nanotechnology*, RSC Pub., Cambridge, 2012.
9 T. K. Gupta, M. Choosri, K. Varadarajan and S. Kumar, *J. Mater. Sci.*, 2018, **53**, 7939–7952.
10 A. Rosehr, D. Griebe and G. A. Luinstra, *Compos. Sci. Technol.*, 2018, **156**, 28–38.
11 C. Zhang, A. Li, Y. H. Zhao, S. L. Bai and Y. F. Zhang, *Composites, Part B*, 2018, **135**, 201–206.
12 Y. L. Li, S. J. Wang, Q. Wang and M. Xing, *Composites, Part B*, 2018, **133**, 35–41.
13 M. A. Rafiee, J. Rafiee, I. Srivastava, Z. Wang, H. Song, Z. Z. Yu and N. Koratkar, *Small*, 2010, **6**, 179–183.
14 G. L. Li, Z. Zheng, H. Möhwald and D. G. Shchukin, *ACS Nano*, 2013, **7**, 2470–2478.
15 S. Yang, J. Wang, W. Mao, D. Zhang, Y. Guo, Y. Song, J.-P. Wang, T. Qi and G. L. Li, *Colloids Surf., A*, 2018, **55**, 18–26.
16 J. P. Wang, J. K. Wang, Q. Zhou, Z. Li, Y. Han, Y. Song, S. Yang, X. Song, T. Qi, H. Möhwald, D. Shchukin and G. L. Li, *Macromol. Mater. Eng.*, 2018, **303**, 1700616.
17 A. Marquez, J. Uribe and R. Cruz, *J. Appl. Polym. Sci.*, 1997, **66**, 2221–2232.
18 G. Astaluta and G. Sarti, *Polym. Eng. Sci.*, 1978, **18**, 388–395.
19 J. R. Nelson, *Fuel*, 1983, **62**, 112–116.
20 R. J. Albalak, M. S. Capel and E. L. Thomas, *Polymer*, 1998, **39**, 1647–1656.
21 H. Mencer and Z. Gomzi, *Eur. Polym. J.*, 1994, **30**, 33–36.
22 M. M. Caruso, D. A. Delafuente, V. Ho, N. R. Sottos, J. S. Moore and S. R. White, *Macromolecules*, 2007, **40**, 8830–8832.
23 R. P. Wool, *Soft Matter*, 2008, **4**, 400–418.
24 P. P. Wang, S. Lee and J. P. Harmon, *J. Polym. Sci., Part B: Polym. Phys.*, 1994, **32**, 1217–1227.
25 M. M. Caruso, B. J. Blaiszik, S. R. White, N. R. Sottos and J. S. Moore, *Adv. Funct. Mater.*, 2008, **18**, 1898–1904.
26 J.-C. Hsu, W. Cao, F. Yang, T.-J. Yang and S. Lee, *Phys. Chem. Chem. Phys.*, 2017, **19**, 7359–7369.
27 K. Shah, D. Vasileva, A. Karadaghy and S. Zustiak, *J. Mater. Chem. B*, 2015, **3**, 7950–7962.
28 J. Abraham, H. J. Maria, S. C. George, N. Kalarikkal and S. Thomas, *Phys. Chem. Chem. Phys.*, 2015, **17**, 11217–11228.

29 O. Starkova, S. Buschhorn, E. Mannov, K. Schulte and A. Aniskevich, *Eur. Polym. J.*, 2013, **49**, 2138–2148.
30 M. T. Kim, K. Y. Rhee, I. Jung, S. J. Park and D. Hui, *Composites, Part B*, 2014, **63**, 61–66.
31 J. P. Harmon, S. Lee and J. C. M. Li, *J. Polym. Sci., Part A: Polym. Chem.*, 1987, **25**, 3215–3229.
32 C. B. Lin, S. Lee and K. S. Liu, *Polym. Eng. Sci.*, 1990, **30**, 1399–1406.
33 T. Kuila, S. Bose, A. K. Mishra, P. Khanra, N. H. Kim and J. H. Lee, *Prog. Mater. Sci.*, 2012, **57**, 1061–1105.
34 L. R. Radovic, C. V. Mora-Vilches, A. J. Salgado-Casanova and A. Buljan, *Carbon*, 2018, **130**, 340–349.
35 A. C. Ferrari, J. Meyer, V. Scardaci, C. Casiraghi, M. Lazzeri, F. Mauri, S. Piscanec, D. Jiang, K. Novoselov and S. Roth, *Phys. Rev. Lett.*, 2006, **97**, 187401.